

Three-dimensional Simulation of a Fire-Resistance Furnace

S. WELCH¹, P. RUBINI

School of Mechanical Engineering
Cranfield University, Cranfield
Bedfordshire, MK43 0AL

S. Welch, P.A. Rubini.

"Three dimensional simulation of a fire resistance furnace".
Proceedings of 5th International Symposium on Fire Safety Science,
Melbourne, Australia, March 1997,
International Association for Fire Safety Science, pp. 1009-1020,
ISBN 4-9900625-5-5.

ABSTRACT

The fire resistance "rating" of a building component or element is determined by its performance in a standard furnace test, for example ISO 834 and ASTM E119. For these "ratings" to be meaningful it is important that specimens be subject to the same standard test wherever it may be conducted. However, existing methods only standardise on a furnace thermocouple temperature-time curve and there are substantial differences in the design of standard furnaces both nationally and internationally. There is therefore considerable variation in perceived fire resistance performance. This paper presents the first application of Computational Fluid Dynamics to the simulation of a full-size fire-resistance furnace following the ISO 834 prescribed time-temperature curve. Results are presented from an investigation into the thermal characteristics of a generic fire resistance furnace. The results illustrate that, whilst following the standard, considerable spatial and temporal variations exist in both incident radiative and convective heat flux to the test specimen. Although no comparison with experimental data is presented at this time, the results illustrate the potential contribution of CFD simulations to assist in the current discussions regarding harmonisation of the fire resistance test.

KEYWORDS: CFD, field modelling, SOFIE, heat transfer, fire resistance test, furnace harmonisation

NOMENCLATURE

c_p	- specific heat capacity ($\text{J kg}^{-1} \text{K}^{-1}$)	Re	- Reynolds number (-)
$conv$	- convection	T	- thermocouple metal temperature (K)
D	- cylinder diameter (m)	T_g	- local gas temperature (K)
h	- heat-transfer coefficient (W K^{-1})	V	- velocity (m s^{-1})
k	- thermal conductivity ($\text{W m}^{-1} \text{K}^{-1}$)	dt	- small time interval
Nu	- Nusselt number (-)	ϵ	- emissivity of the thermocouple (-)
Pr	- Prandtl number (-)	μ	- coefficient of viscosity ($\text{kg m}^{-1} \text{s}^{-1}$)
q	- heat flux (W m^{-2})	ρ	- density (kg m^{-3})
rad	- radiation	σ	- Stefan Boltzmann constant ($\text{W m}^{-2} \text{K}^{-4}$)
R	- resistivity (Q m^{-1})		

¹ Now at Fire Research Station, Garston, Watford, WD2 7JR

INTRODUCTION

Furnace testing is a **statutory** requirement in most countries for the assessment of the **fire** resistance of building elements such as walls, beams and columns. Almost all countries have standardised test methods, which, though similar to an internationally accepted standard, are specific to each individual country. The national standards are similar to the ISO-standard 834, first published in 1975 [1]. The standard represents a common denominator of the national standards of each of the participating countries.

There are a number of different **types** of test furnaces including furnaces for horizontal items such as beams, floors and bulkheads and furnaces for vertical items such as walls and doors [2]. Although parts of a standardised method, the design and characteristics for the furnaces vary. Since a furnace represents a considerable investment, it has not been realistic to require that existing furnaces should be modified to conform to a single design. Consequently, various furnaces may expose the specimen to heating conditions **that** differ even though the same standardised test method is employed. The standardised method prescribes a time-temperature relationship that should be followed during a test in which the temperature is that recorded by thermocouples placed in the furnace near the specimen.

The thermal performance of fire-resistance furnaces has been investigated by a number of authors over the last two decades, for example [3-6]. In particular, detailed analyses were presented in [3,4]. However, in all previous analyses, considerable simplifying assumptions were necessary to either reduce the computations to a tractable form or to approximate unknown parameters. A common assumption of the cited studies is that the furnace atmosphere may be treated as homogenous at a constant temperature equal to the controlling time-temperature relationship. In addition, the furnace walls are also assumed to exhibit uniform temperature distributions. Any non-uniformities due to the internal fluid dynamic behaviour of the furnace have been necessarily ignored.

The **three-dimensional** geometry of the furnace, containing a complex, spatially and temporally varying, three-dimensional, turbulent, combusting flow-field has in the majority of all earlier studies been reduced to a one-dimensional heat-transfer equation yielding the total heat flux to the specimen and the one-dimensional temperature distribution across the specimen. Whilst such methods have provided valuable insight into the dominant modes of heat transfer and performance of furnaces, they are limited in capability when more detailed spatial information is desirable.

CFD is now commonly used for fire science modelling, see for example [7]. Often referred to **as field modelling**, typical applications include smoke movement and heat transfer, in circumstances where traditional zone models are inappropriate. Field model predictions of fires in **enclosures** play an increasingly important role **in** the assessment of widely differing fire hazard scenarios.

One of the principal advantages of Computational Fluid Dynamics is that many different designs may be compared, often **at much** lower cost than equivalent experimental procedures. CFD offers a tool that may be used to assess and compare the variety of different fire test furnaces, providing a detailed description of the heat transfer regime actually being experienced by the test specimen. Therefore CFD may be used to compare different furnaces with respect to their **conformance** of an agreed furnace fire test standard. Surprisingly, to date there have been no previously published examples illustrating the use of CFD to simulate fire-resistance furnaces, though application to industrial furnaces is now well-established [8,9]. This paper presents the first application of Computational Fluid Dynamics to the simulation of a full-size fire-resistance furnace following the ISO 834 prescribed time-temperature curve.

In practice, thermocouple control is achieved by matching the measured thermocouple temperatures to the ISO curve. However, since thermocouples re-radiate heat, they adjust themselves to the temperature at which there is a balance between the heat transferred by convection and the net radiative transfer (neglecting other minor effects) [3]. This may be considerably below the local gas temperature, by up to 100 K and it is essential **to** simulate this behaviour if any meaningful comparison between predictions and actual operation is to be achieved. In the current work, the thermocouple temperature has been simulated by carrying out a detailed radiation calculation over the thermocouple beads at the exact thermocouple locations in the furnace.

NUMERICAL PROCEDURE

The numerical predictions were carried out using **SOFIE**, (Simulation Of Fires In Enclosures), a **CFD** code written at **Cranfield** University with support from a number of European fire research laboratories, including the Fire Research Station (UK), SP Boras (Sweden), **VTT** (Finland), **CSTB** (France).

The development of **SOFIE** was driven by two principal objectives. **Firstly**, to develop a field-modelling code specifically for the prediction of fires in buildings, which incorporates the core features of current commercially-available, **general-purpose**, fluid dynamic codes; secondly to develop within the code a range of fire-specific features to enable prediction of more complex fire phenomena not normally accessible to general-purpose **CFD** codes. Examples of these latter features include fire growth and spread, toxic emissions and dispersion, fire-water spray interaction.

SOFIE employs a finite volume pressure correction procedure to solve the governing density weighted Navier-Stokes equations in a general **curvilinear** coordinate system. The standard k-e turbulence model is employed with buoyancy **modifications**. Combustion is accounted for by assuming that the rate of heat release is limited by turbulent mixing of the fuel and **oxidant**, as modelled by an eddy breakup combustion model. A more detailed description of **SOFIE** is available in [10].

The specific heats of individual components (fuel, oxidant, products) are described by fourth-order **polynomials**, heat release is represented by a balance between heats of formation. Additional transport equations are solved for mixture **fraction**, fuel mass fraction and enthalpy. These equations are based on a scalar transport equation with the following modified source terms: mixture fraction - source equals zero; fuel mass fraction - source equal to rate of **fuel** consumption given by the eddy breakup combustion model; **enthalpy** equation - source includes the net energy absorbed or emitted by radiation and the rate of heat release prescribed by the combustion model. Each individual scalar transport equation is solved in addition to those for momentum, continuity and the turbulence model.

Heat transfer to the internal walls of the furnace is modelled via a predicted heat transfer coefficient for convection based upon a conventional '**law-of-the-wall**' description and a defined emissivity for radiation. Heat transfer through the solid walls of the furnace and through the specimen is modelled by solving the enthalpy equation in these regions with only conduction. Heat transfer from the external walls of the furnace to the surrounding atmosphere is modelled by prescribing a constant ambient temperature and an external heat **transfer** coefficient.

Thermal radiation within the furnace is modelled using a deterministic ray tracing approach based upon the discrete transfer algorithm [11]. This technique employs a ray tracing procedure whereby individual *pencils* or bundles of rays are traced from each participating solid surface in the physical enclosure. Each surface in this context is an individual face of a control volume described by the underlying **CFD** grid. A user-specified number of rays, distributed over the unit hemisphere, are traced from each surface. The rays pass through gaseous volumes, taken to be the **CFD** grid control volumes, in which they may absorb or emit thermal energy. On eventually arriving at an opposing surface the resultant thermal energy is either absorbed or reflected as determined by the local emissivity. In the present calculations, a constant gas absorption coefficient was used throughout the furnace. More accurate procedures could be employed whereby the absorption coefficient is determined from individual concentrations of the local gaseous components, temperature and optical path length, see for example [12,13].

Thermocouple simulation

The temperature recorded by a furnace thermocouple depends upon several factors. Heat is transferred to the metal by convection and radiation and heat is lost through re-radiation and conduction along the thermocouple wires. Usually, conduction can be neglected and transient heating effects **can** also be ignored since the characteristic times are small in comparison with the running times. Thus, only the convection and radiation effects need be considered. The thermocouples will adjust themselves to the temperature which provides a balance between the heat induced by convection and the heat given off by radiation, represented by the

following equation:

$$h (T_g - T) = \sigma \epsilon T^4 - \Sigma q_{rad}$$

where, h is the heat transfer coefficient of between the metal and the gas, T_g is the local gas temperature, T is the thermocouple metal temperature, σ is the **Stefan-Boltzmann** constant, ϵ is the **emissivity** of the thermocouple and Σq_{rad} is the incident radiative flux to the thermocouple. The heat transfer coefficient in **turn** may be obtained from a **Nusselt-number** correlation for cylinders [14]:

$$h = \frac{k Nu}{D}$$

where:

$$Nu = 0.42 Pr^{0.2} + 0.57 Pr^{0.33} Re^{0.5}, \quad Pr = \frac{\mu c_p}{k}, \quad Re = \frac{\rho U D}{\mu}$$

Also, the metal emissivity is a function of temperature and resistivity as follows [14]:

$$\epsilon = 2.37 \times 10^{-2} (TR)^{\frac{1}{2}} - 6.32 \times 10^{-3} TR + 2.12 \times 10^{-5} (TR)^{\frac{3}{2}} - 6.07 \times 10^{-6} (TR)^2$$

Here, R is the wire resistivity in Ωm^{-1} .

In **SOFIE**, all of these parameters are available, allowing determination of the thermocouple temperature by a simple numerical method.

FURNACE SIMULATION

A generic **fire-resistance** test furnace was modelled as illustrated in figure 1 (a symmetric half is shown). This is a wall furnace with a total of fourteen burners arranged opposite each other in two sets of seven. The wall to the left of the burners in the diagram is the test specimen. Two sets of four exhausts are set opposite to the specimen wall and adjacent to each burner end-wall. The internal dimensions of the test specimen are 3.08 m high by 3.06 m wide, and the depth of the furnace is 0.93 m, yielding a furnace volume of 8.76 m^3 .

The furnace was assumed to be constructed from ceramic walls, approximately 150 mm thick. In the current simulation, a 50 mm steel sheet was used as the test specimen. The relevant physical parameters for the **SOFIE** simulation are summarised below.

The steel test specimen has the following properties [4]:

• thermal conductivity	42.0 $W m^{-1} K^{-1}$
• specific heat capacity	530 $J kg^{-1} K^{-1}$
• density	7850 $kg m^{-3}$
• surface emissivity	0.80

The ceramic furnace walls have the following properties:

• thermal conductivity	0.34 $W m^{-1} K^{-1}$
• specific heat capacity	1000 $J kg^{-1} K^{-1}$
• density	880 $kg m^{-3}$
• surface emissivity	0.90

According to the ISO standard, 9 bare **18-gage** thermocouples were used, located 100 mm from the specimen surface. Three were positioned on the furnace centreline, and three offset 0.7 m towards the burners. In each case, the vertical positions were 0.52 m, 1.43 m and 2.34 m from the floor of the furnace. A further nine thermocouples are positioned on the hot-side specimen surface at adjacent locations. The material specification is as follows [15,16]:

• material	Chromel-Alumel
• resistivity	10.58 $\mu\Omega \text{ m}^{-1}$ @ 20°C
• thickness	1.5 mm

The **fuel** was taken to be pure methane, with a heat of combustion equal to 50 MJ kg⁻¹. A **stoichiometric** mixture was used throughout. The absorption coefficient of the furnace gases was assumed constant and equal to 0.2 m⁻¹.

A symmetrical half of the furnace was modelled using a computational grid of 21 x 24 x 54 nodes, giving a total of 27216 cells. Two nodes were placed across each wall, including the specimen. A mirror symmetry plane was used to reduce both memory requirements and computational time. The simulation was run for a one hour transient test.

RESULTS

A selection of results from the simulation are shown in figures 2-12. Figures 2-7 illustrate the development of combustion and the heat transfer behaviour during the **full** one hour test using parameters averaged over either the whole furnace or one of the furnace **walls**. Figures 8 and 9 present the spatial and temporal temperature variation at the thermocouple locations during the whole test period. Finally, figures 10-14 provide a more detailed description of **the** spatial variation of the heat transfer process over the specimen face at the end of the test.

Combustion in the furnace was controlled by varying the supply rate of the fuel-air mixture in order to achieve a match between the ISO temperature curve and the average temperature reading of the thermocouples. Figure 2 shows the variation of flow rate and the resulting temperature curve; an acceptable degree of accuracy has been achieved, with the maximum error being less than **50K**. Figure 2 also gives the predicted gas temperature averaged over **the** whole furnace. As expected, this is significantly higher than the predicted average thermocouple temperatures. In fact, the latter averaged **65K** lower than the local gas temperatures **at the end of the test**.

Figure 3 shows the variation of the face temperatures averaged over the whole of the steel specimen wall and the whole of the ceramic exhaust wall opposite. Due to its low thermal inertia ($Vkpc = 547 \text{ J m}^{-2} \text{ s}^{-1/2} \text{ K}^{-1}$), the ceramic face temperature is very high, reaching **1112K** at the end of the test. This compares with the final bulk gas temperature of 1338K. It is noticeable that the shape of the ceramic and gas temperature curves is very similar, and a fairly constant temperature difference of **200K** is maintained throughout the test. The steel, on the other hand, has a high thermal inertia ($vkpc = 13220 \text{ J m}^{-2} \text{ s}^{-1/2} \text{ K}^{-1}$). It can therefore absorb heat much more effectively and the surface temperature **consequently** rises much more slowly. Nevertheless, at the end of the test, the specimen average surface temperature has reached 962K, only **150K below** that of the opposite ceramic wall.

Figures 4-7 present a breakdown of the heat transfer behaviour during the test. Figures 4 and 5 show the variation of the total **convective** heat flux and the average heat transfer coefficient on the specimen and exhaust wall respectively. The calculated average of the convective heat transfer coefficient is fairly constant at around 6 W m² K⁻¹ on both walls. The average convective heat flux to the specimen peaks at about 4 kW m⁻² early in the test, and drops to about 2 kW m⁻² at the end. The steady fall is due to the progressive narrowing of the gap between the surface and the gas temperatures (see figure 3 above). In the case of the ceramic exhaust wall, the **convective** heat flux is lower throughout and fairly constant at between 1 and 1.6 kW m⁻². This arises from the lower temperature difference between this **wall** and the furnace gases.

Figures 6 and 7 show the breakdown of the radiation heat transfer to the specimen and exhaust walls. At both walls, the average incident radiative flux rises progressively during the test, due to the increasing gas temperatures. The peak radiative flux on the specimen is 105.8 kW m^{-2} compared with 94.5 kW m^{-2} on the exhaust wall. This difference is probably due to the fact that there are eight burners adjacent to the specimen wall, but **only** six beside the exhaust wall.

A much more distinct difference is observed in the radiative fluxes leaving the walls. For the specimen, the average emitted flux rises slowly as the face temperature rises, and it reaches a peak value of 55.8 kW m^{-2} at the end of the test. This is just over half of the average incident flux. However, on the exhaust wall the emitted flux mirrors the incident flux very closely, and the final level of 90.5 kW m^{-2} is 96% of the incident flux. This is of course due to the much higher face temperature of the ceramic material. Consequently, the net radiative flux to the exhaust wall is on average less than 10% of that to the specimen.

Table 1 provides summary data for the total heat transferred to the furnace walls during the full one hour test. It can be seen that the heat load on the specimen is over 10 times as high as that on the ceramic exhaust wall. Also, convective heat transfer is of relatively little significance for the specimen, being only 5.3% of the total. These differences are in accord with expectations, since the steel specimen has a much higher thermal inertia, such that even with equal surface temperatures, the steel absorbs heat more rapidly than the ceramic.

Furnace surface	$\Sigma q_{conv} \delta t$ (MJ m ⁻²)	$\Sigma q_{rad} \delta t$ (MJ m ⁻²)	$\Sigma q_{conv} \delta t /$ $\Sigma q_{rad} \delta t$ (%)	$\Sigma q_{tot} \delta t$ (MJ m ⁻²)	$\Sigma q_{tot} \delta t / \sqrt{k\rho c}$ (s ^{-1/2} K)
Specimen wall	9.3	173.7	5.3	183.0	13.8
Exhaust wall	4.6	13.4	34.1	18.0	32.9

Table 1

The final column in the table is the normalised heat load, where the total heat load has **been** normalised by the thermal **inertia** of the material [4]. This shows that despite the much greater heat load on the steel specimen, **the** normalised heat load is only about 40% of that on the ceramic exhaust wall. The large difference in this parameter is consistent with **Harmathy's** calculated values for gases with low absorption coefficients [4]. It suggests that in this type of furnace, there is some interaction between the specimen and the furnace walls, though it has normally been neglected in furnace calculations [3,4]. In order to circumvent the problem of poor test **reproducibility**, **Harmathy** recommends that test **furnaces** are heated by gases of high radiation potential, i.e. near-black gases [4].

Figures 8 and 9 show the variation in the temperatures of the free and face thermocouples with time. The legend refers to the thermocouples on the furnace centreline as 'Mid' and those offset towards the burners as 'Edge'. The second term refers to the vertical height in the **furnace**. It can be seen that there is a considerable variation in each set of values, and the final maximum differences are **335K** and **96K** for the free and face thermocouples respectively. The temperatures recorded on furnace centreline ('Mid' values) are generally lower than the levels nearer the burners. This is because the latter are nearer to the region of most intense combustion in the burner plumes.

Figures 10-14 provide a more detailed description of the spatial variation of the heat transfer process at the end of the test. In these figures, various parameters are plotted over a symmetric half of the specimen face. The positions of the burners in the right-hand wall are indicated with the labels 'L' and 'R' for burners shown in figure 1 on the left and the right respectively, and the exhaust holes are also shown.

Figure 10 shows that the face temperature varies considerably over the surface of the specimen. The temperature peaks at over **1100K** in a region towards the middle of the specimen adjacent to the burner plumes, and steadily falls off towards the edges. The peak region is offset slightly above the centre of the burner region due to the effects of buoyancy. Whilst the face thermocouples recorded a final maximum difference of **96K** (figure 9), the actual difference between the central **peak** and the edge regions is over **350K**. In fact, the difference recorded by the thermocouples will be sensitive to the exact nature of the **flowfield**.

Figure 11 shows the predicted **convective** heat flux (defined as negative going from fluid to solid). Again, a central peak region is visible, offset slightly higher than the peak temperature region. Secondary peaks are visible near the edges of the specimen wall, particularly at the top of the furnace. These arise because the lower face temperatures in these regions give a greater temperature differential between the gas and the wall to drive the heat transfer.

Figure 12 shows the incident radiative heat transfer. The peak value of 139.5 kW m^{-2} is found near the centre of the **wall**, which is the area adjacent to the most intense region of combustion in the burner plumes. The levels at the edges of the specimen drop to less than half of the peak value. This indicates that radiation from the gas is dominant, and the effects of radiation from the adjacent walls is relatively unimportant.

The emitted radiative flux shown in figure 13 has a similar distribution to that of face temperature, as expected. Because of the high temperatures in the middle of **the wall**, the effect of the high levels of incident radiation to this region are largely negated. Thus, the net radiative heat transfer (figure 14) shows a much more even **distribution**, with the peak being only about 50% greater than the lowest levels. In this case, there is a small peak towards the middle of the surface, where the incident flux peaks, and high levels are also found near the edges of the specimen, particularly adjacent to the burner **wall**. Again, the reason for these secondary peaks is the higher temperature differential driving the heat transfer in these regions.

Since both the convective and the net radiative flux to the edge regions are higher than average, it might have been expected that the temperature would be higher here. However, during most of the test period the peak heat transfer has been towards the middle of the specimen where the peak incident radiative flux is located. It is only once this region has become hot, that the net radiative transfer reduces and the significantly lower temperatures at the edges lead to a faster rate of temperature rise in this region.

Further work will consider the effect of using fuels whose combustion products have a higher radiation potential. Also, the effect on the thermal response of using different furnace lining and specimen materials will be examined.

CONCLUSIONS

The simulation of combustion in a full-scale **14-burner** fire-resistance furnace with a steel specimen wall has been reported. The results show that there is significant temporal and spatial variation in the thermal load imposed upon the specimen, with a variation of over 350 K across the face of the specimen at the end of the test. Radiation heat transfer is dominant, and particularly so for the steel specimen. Also, because of the relatively low absorption coefficient assumed for methane, significant interaction occurs between the walls and the specimen, contrary to the usual furnace modelling assumptions. Thus, use of a different fuels, specimen materials or furnace linings are all likely to have a marked effect on the overall thermal performance. Since the standard furnace control strategy makes use of an average of the nine thermocouple temperatures, the resulting perceived fire resistance ratings may be poor representations of the real material **properties**. This has important implications for the standardisation of furnace testing. In conclusion, this work has demonstrated that **CFD** techniques have great potential for investigating the thermal **behaviour** of fire-resistance furnaces and may be able to assist in the **harmonisation** of fire-resistance test procedures.

ACKNOWLEDGMENTS

The authors **gratefully** acknowledge the financial support of **BRE/FRS** under contract number EMC 95/42 and their permission to publish this work.

REFERENCES

1. ISO, Fire Resistance Tests - Elements of Building Construction, International Standard **834**, 1975
2. Lie,T.T., "Fire and Buildings", Applied Science Publishers Ltd., London 1972
3. Paulsen ,O.R., Hadvig,S., "Heat transfer in fire test furnaces", J. Fire and Flammability, vol. 8, pp. 423-442, 1977
4. Harmarthy,T.Z., "The fire resistance test and its relations to real world fires", Fire and Materials, vol. 5, no. 3, pp. 112-122, 1981
5. Milke,J.E., "Overview of existing analytical methods for the determination of fire resistance", Fire Technology, vol. 21, no. 1, pp. 59-65, 1985
6. Sultan,M.A., Harmarthy,T.Z., Mehaffey,J.R., "Heat transmission in fire test furnaces", Fire and Materials, vol. 10, pp. 47-55, 1986
7. Cox,G., Kumar,S., "Field modelling of fire in forced ventilation enclosures", Combustion Science and Technology, vol. 52, pp.7-23, 1987.
8. Venturino,M., Rubini,P.A., "Coupled fluid flow and heat transfer analysis of steel reheat furnaces", 3rd European Conference on Industrial Furnaces and Boilers, 18-21 April 1995, Lisbon, Portugal, eds. Leuckel, Collin, Ward, Reis. ISBN 972-8034-02-4
9. Rubini,P.A., Pollard,A., "Three dimensional modelling of a steel reheat furnace". Int. Symp. on Steel Reheat Furnace Technology, August 26-29, 1990, Hamilton, Ontario, Canada, editor F. Mucciardi, ISBN 0-920603-32-7
10. Rubini,P.A., "SOFIE Technical Summary", School of Mechanical Engineering, Cranfield University, Internal Rept. S-1996-1
11. Bressloff,N., Moss,J.B., Rubini,P.A. "Application of a new weighting set for the discrete transfer radiation model". 3rd European Conference on Industrial Furnaces and Boilers. Lisbon, Portugal, 18-21 April 1995. Eds. Leuckel, Collin, Ward, Reis.ISBN 972-8034-02-4
12. Bressloff,N.,Moss,J.B., Rubini,P.A., "Assessment of a differential total absorptivity solution to the radiative transfer equation as applied in the discrete transfer radiation model", Numerical Heat Transfer, Part B: Fundamentals, May, 1996
13. Bressloff,N., Moss,J.B., Rubini,P.A., "CFD predictions of coupled radiation heat transfer and soot production in turbulent flames", to be presented at 26th Int. Symp. Comb., Naples, Italy, August, 1996
14. Hottel,H., Sarofim,A., "Radiative Transfer", McGraw-Hill, 1967
15. Harmarthy,T.Z., Sultan,M.A., "Correlation between the severities of the ASTM E1 19 and ISO 834 fire exposures", Fire Safety Journal, vol. 13, pp. 163-168, 1988
16. GOODFELLOW Catalogue, 1995/6

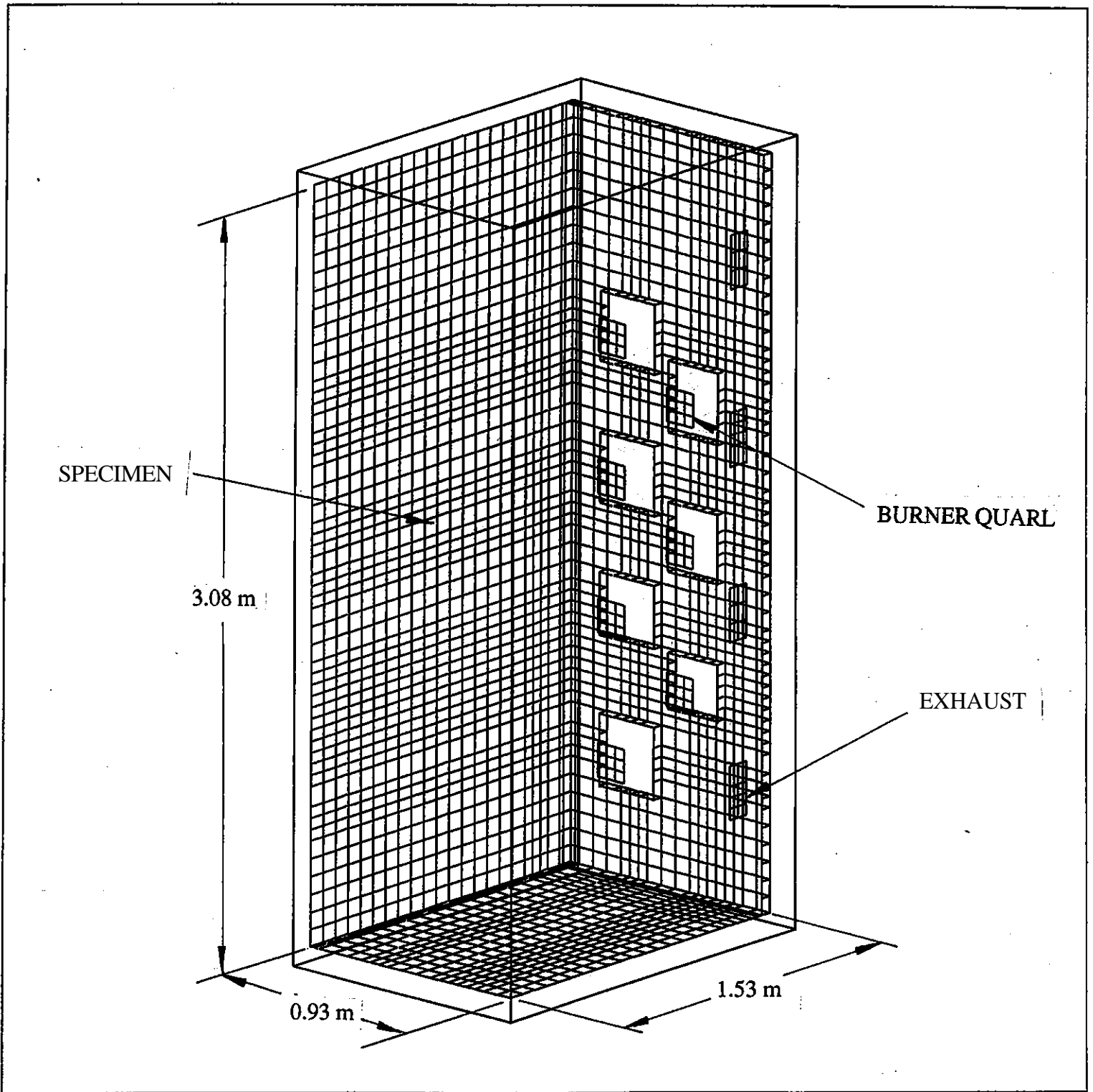


Fig. 1 - Furnace geometry

Temperatures and gas flow rate

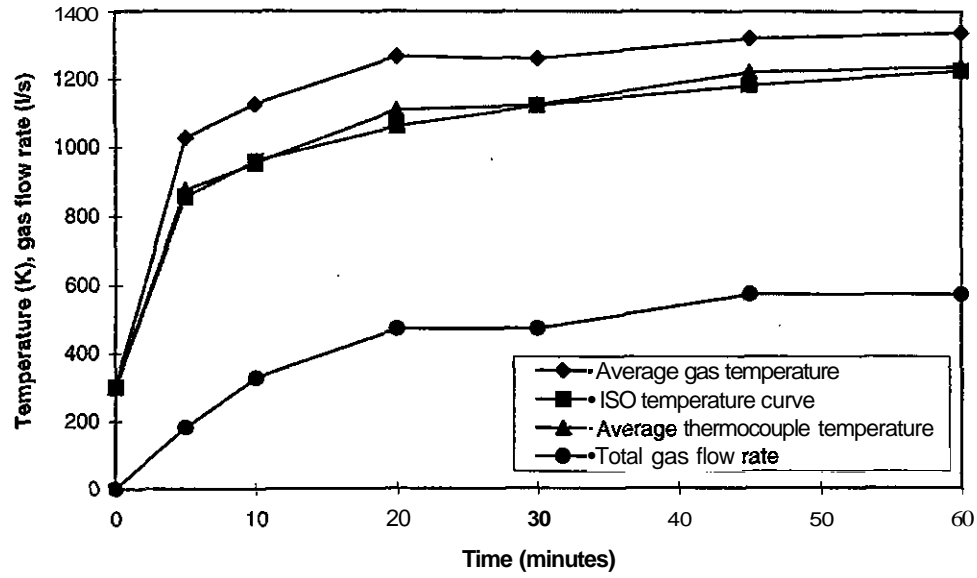


Fig. 2 - Temperatures and gas flow rate

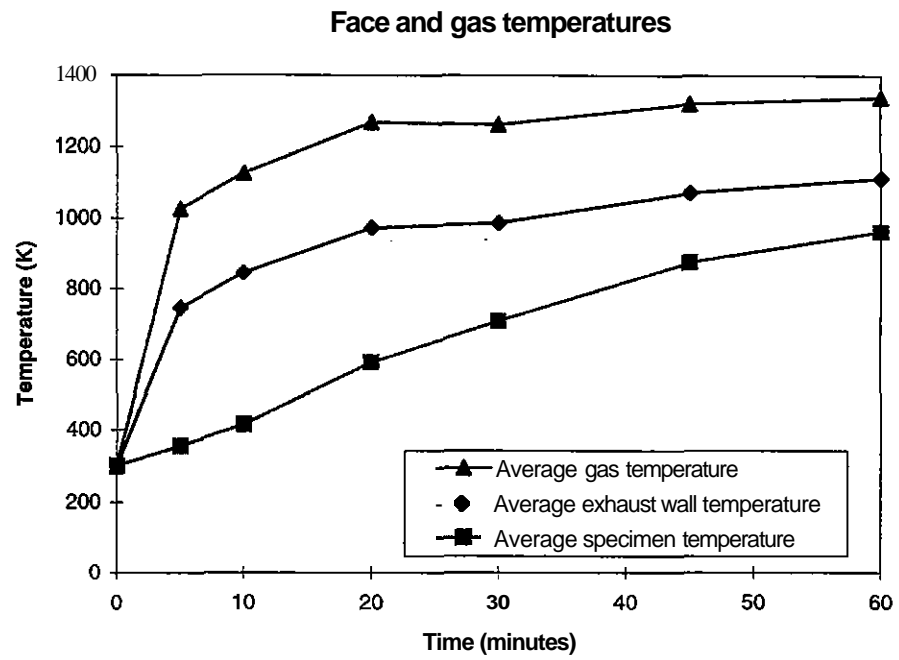


Fig. 3 - Face and gas temperatures

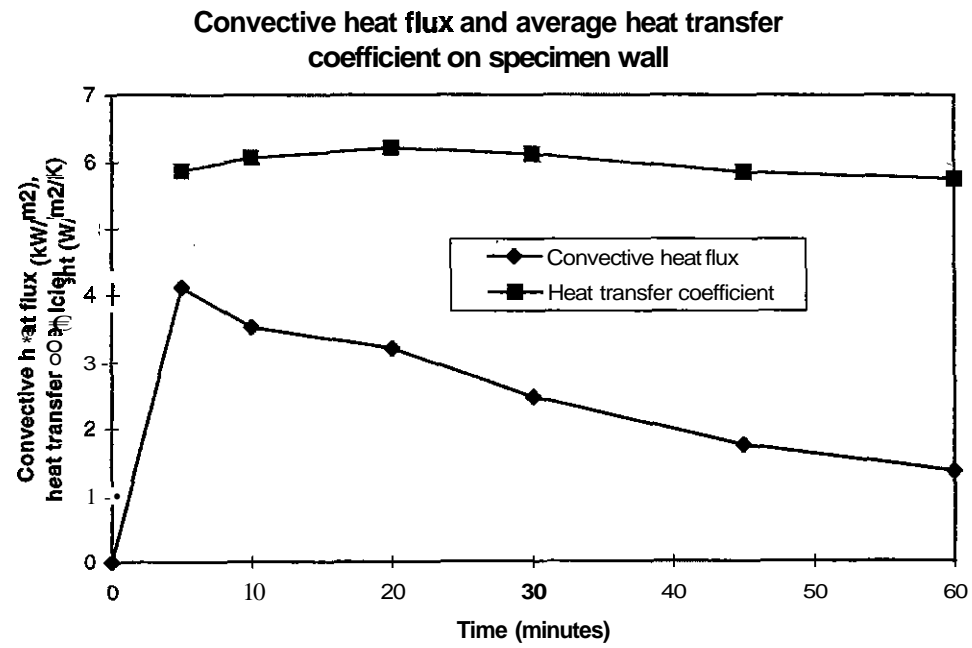


Fig. 4 - Convective heat flux and average heat transfer coefficient on specimen wall

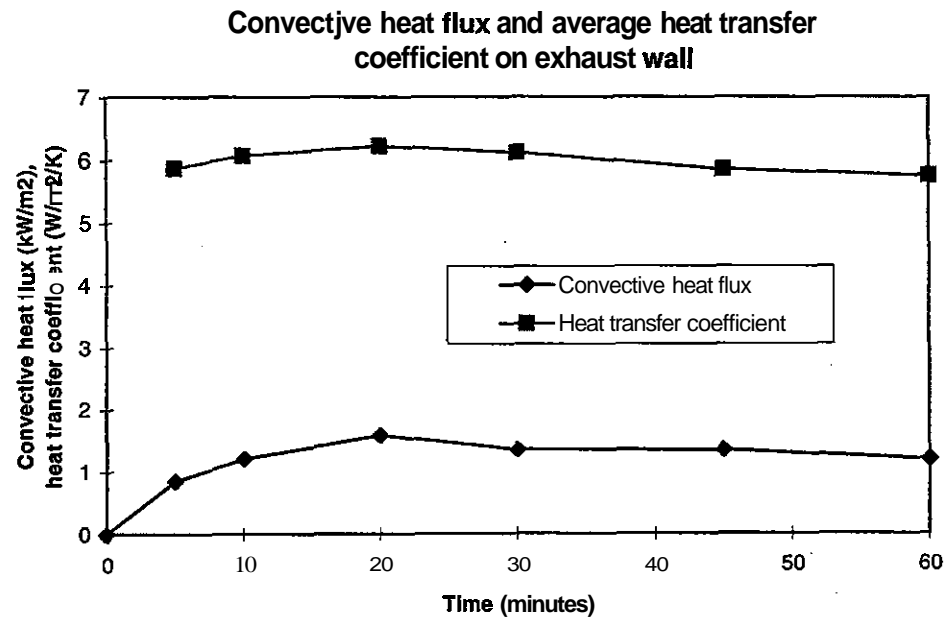


Fig. 5 - Convective heat flux and average heat transfer coefficient on exhaust wall

Radiative fluxes on specimen wall

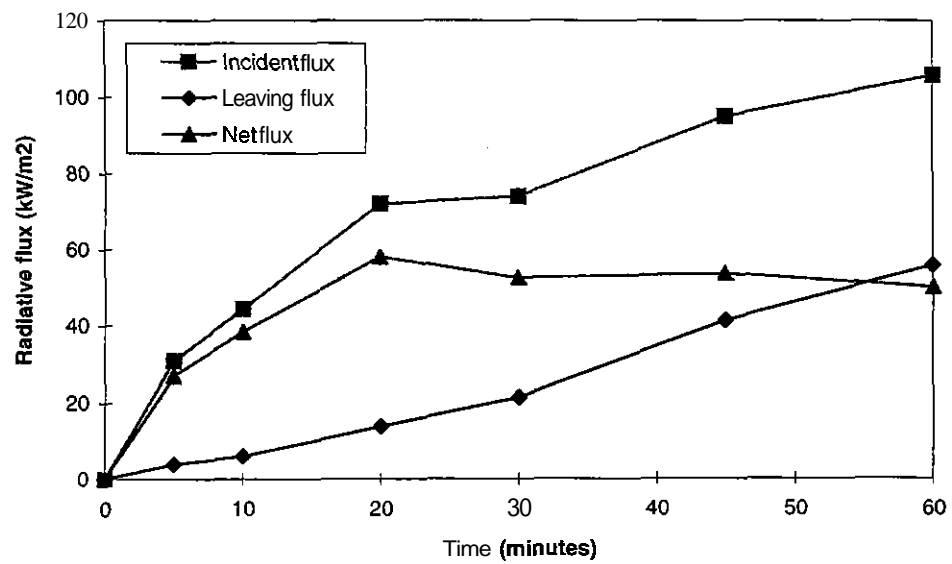


Fig.6 - Radiative fluxes on specimen wall

Radiative fluxes on exhaust wall

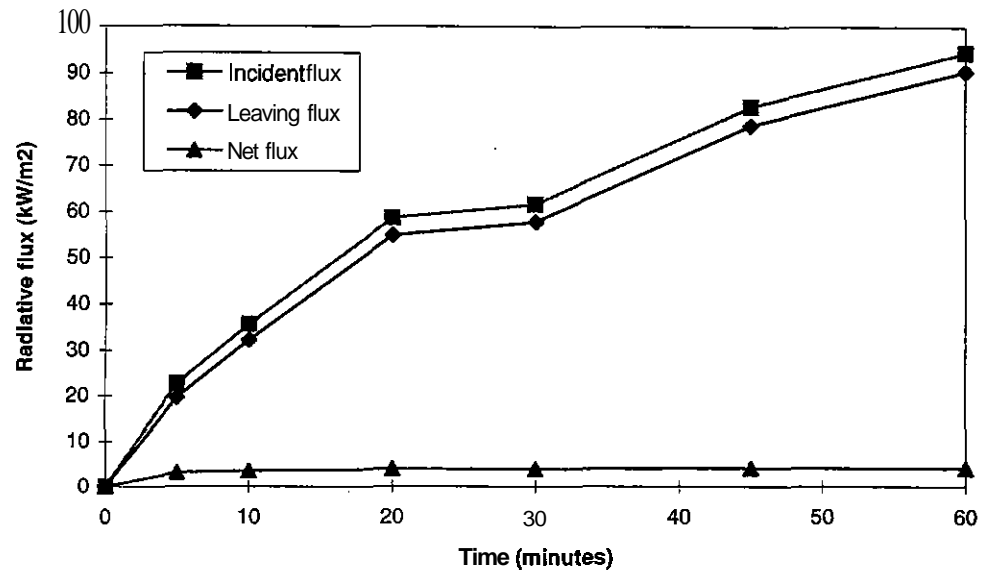


Fig. 7 - Radiative fluxes on exhaust wall

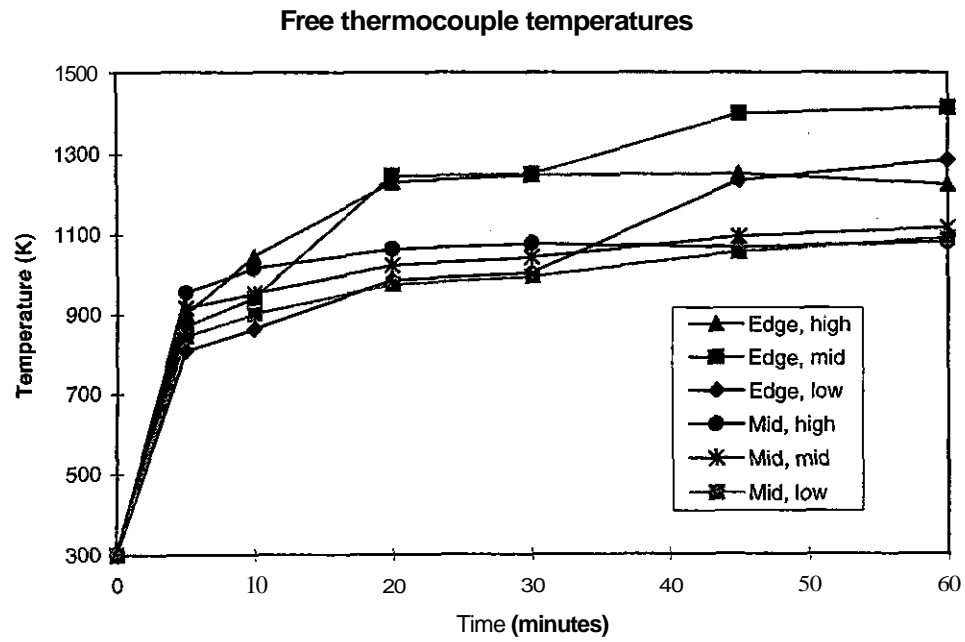


Fig. 8 - Free thermocouple temperatures

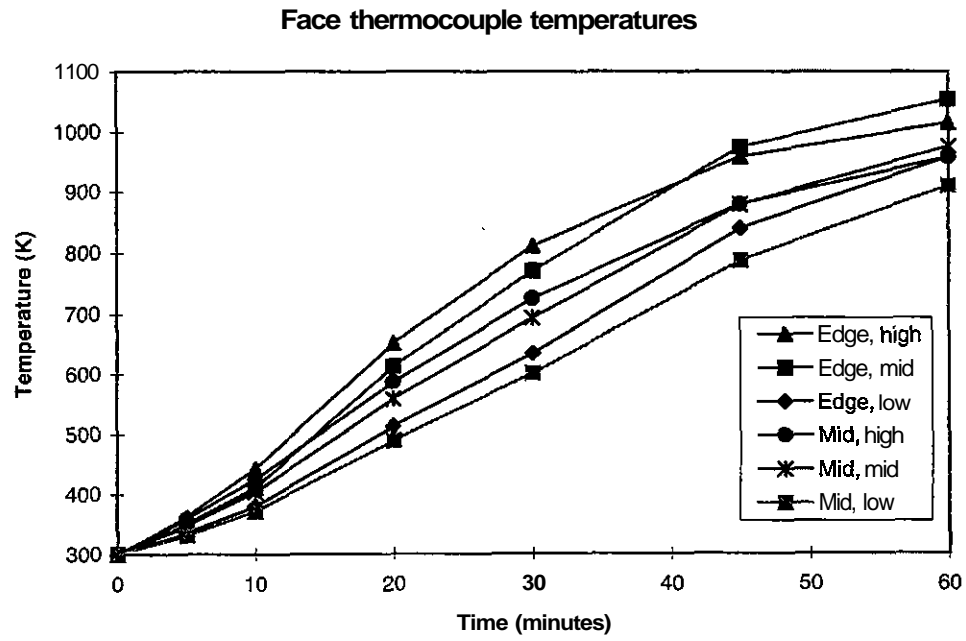


Fig. 9 - Face thennocouple temperatures

Doesn't photocopy well.

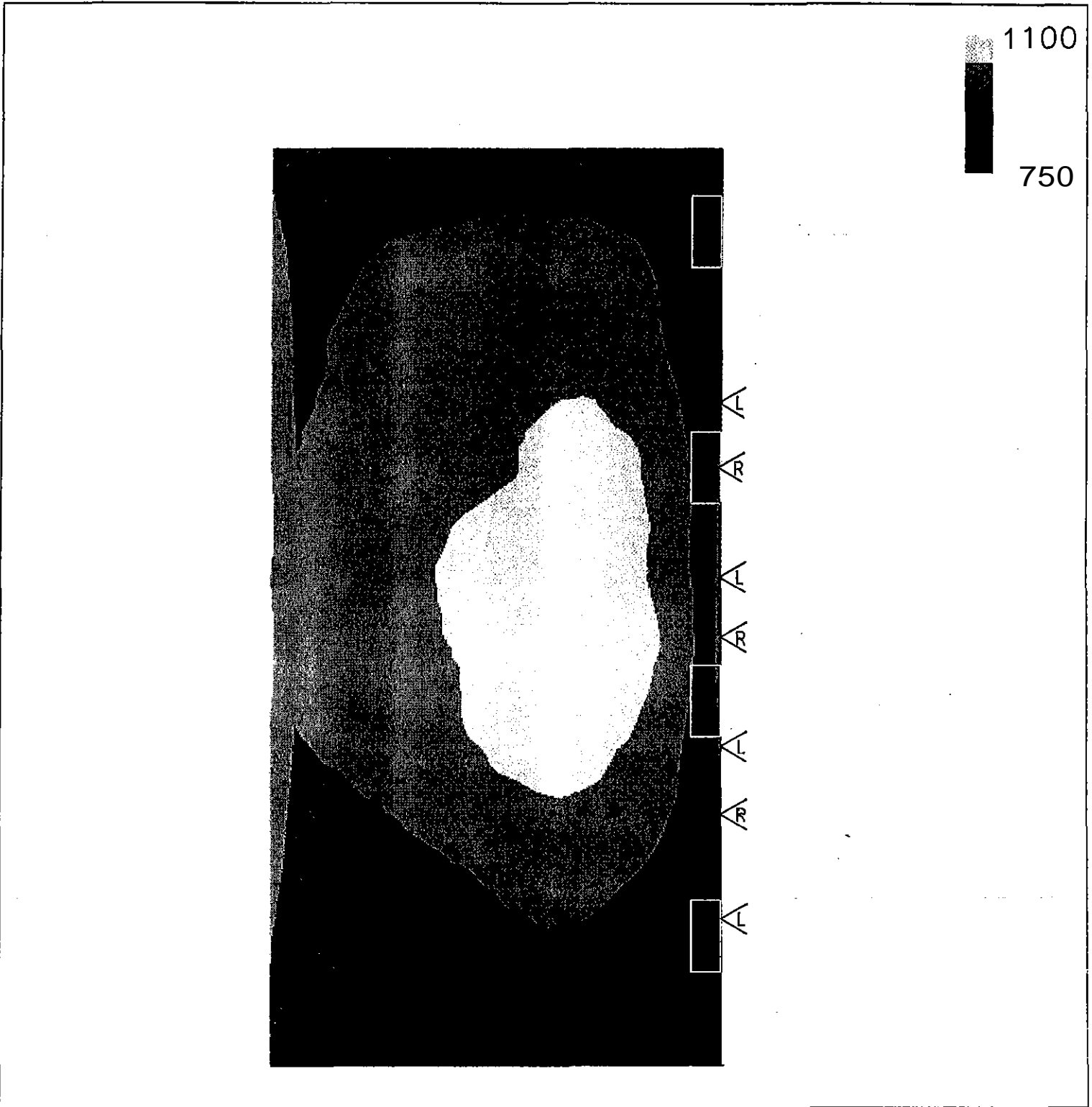


Fig. 10 - Specimen face temperature distribution

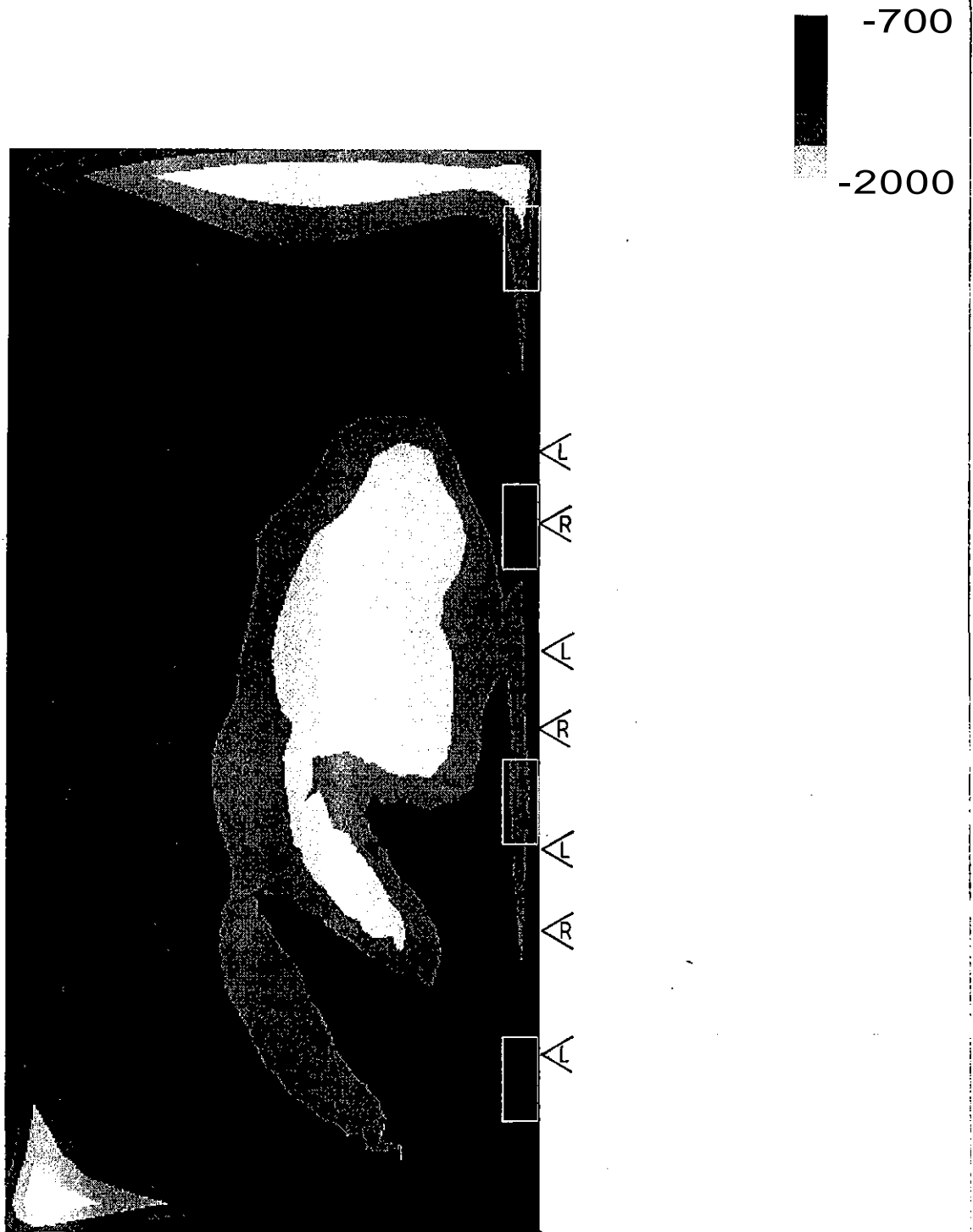


Fig. 11 - Specimen convective heat flux distribution

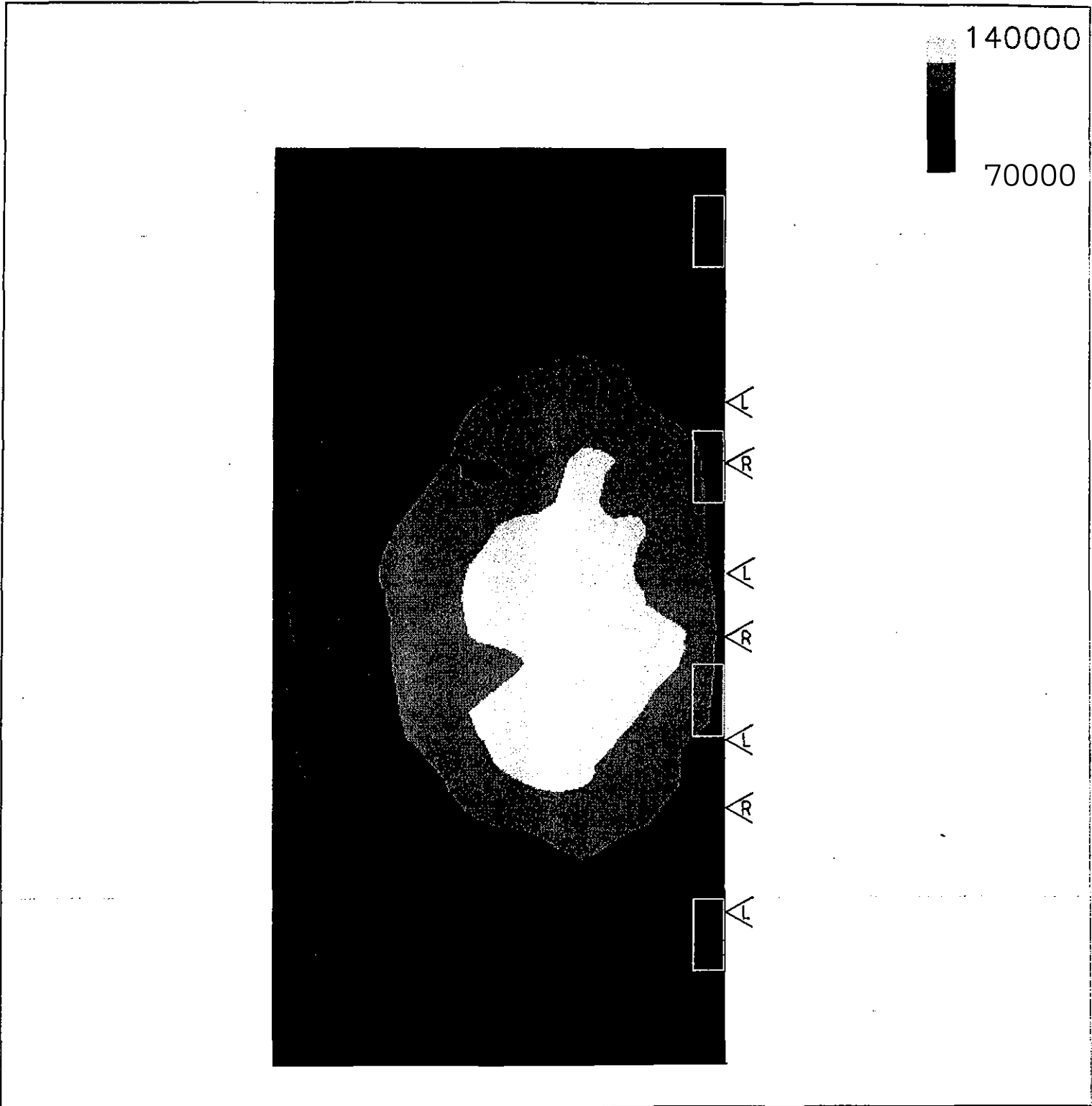


Fig. 12 - Specimen incident radiative flux distribution

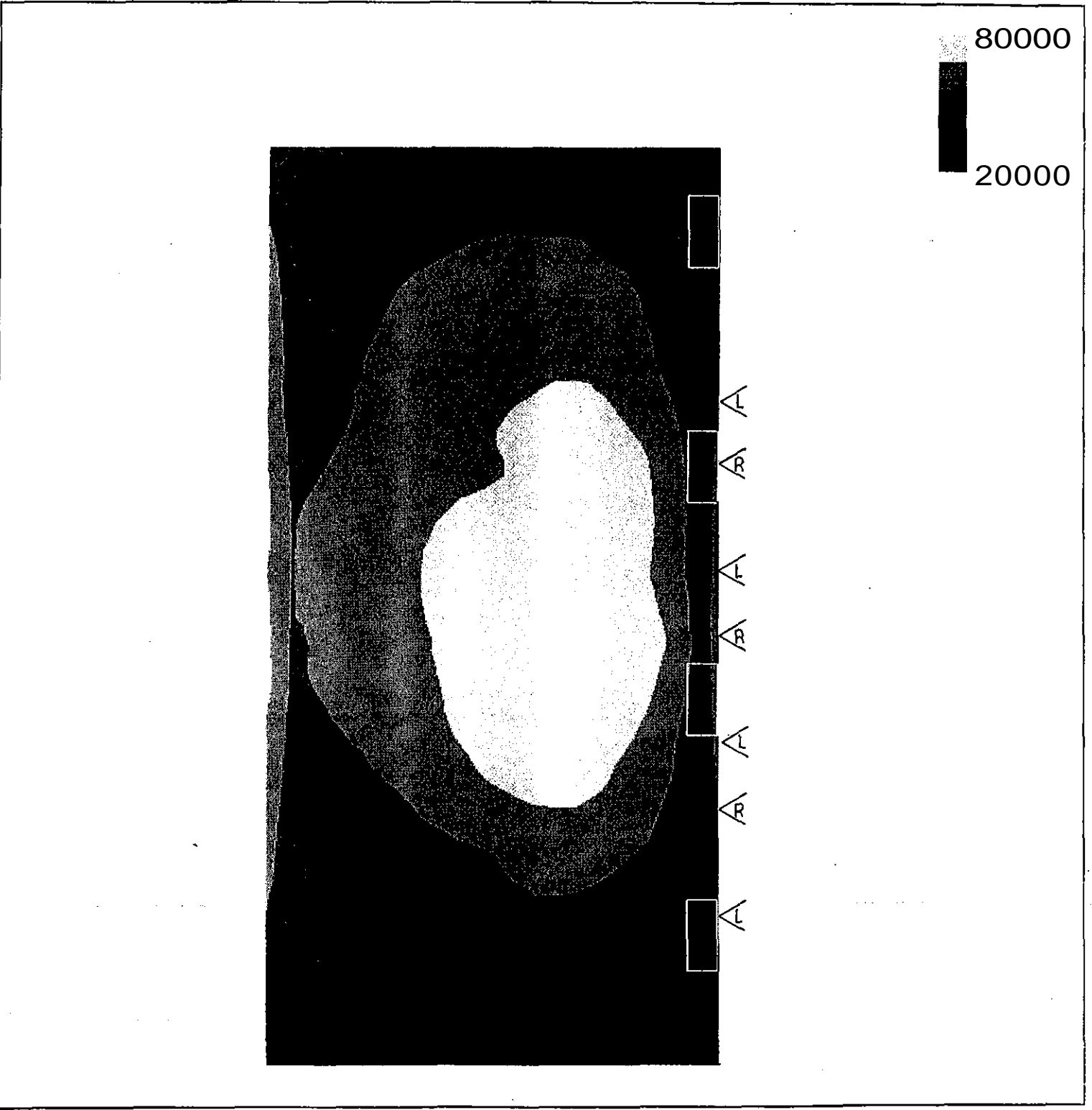


Fig. 13 - Specimen emitted radiative flux distribution

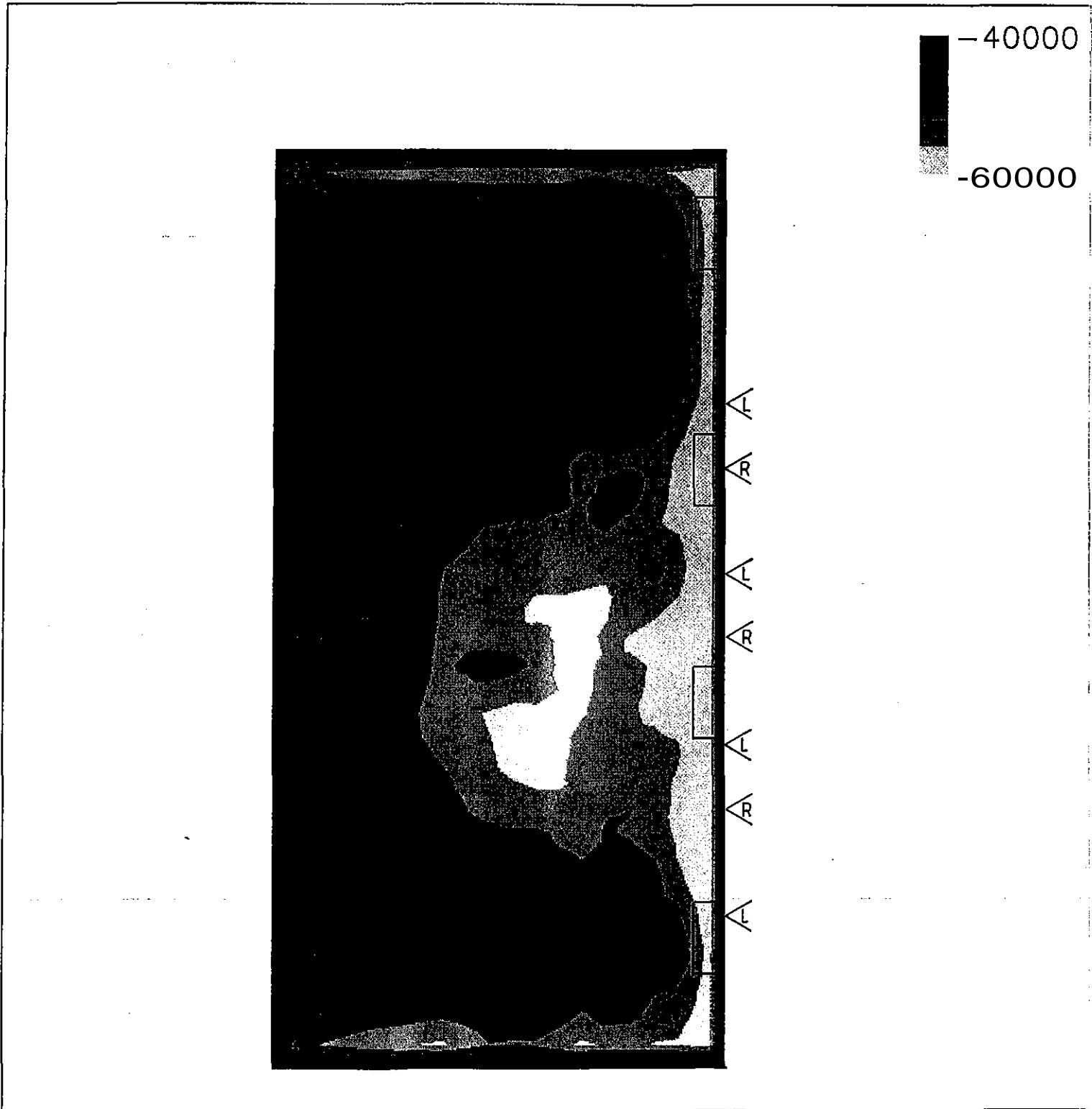


Fig. 14 - Specimen net radiative flux distribution